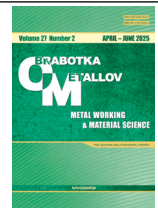




Obrabotka metallov -

Metal Working and Material Science

Journal homepage: http://journals.nstu.ru/obrabotka_metallov







Performance of Y-TZP- Al_2O_3 composite ceramics in dry high-speed turning of thermally hardened steel 0.4 C-Cr (AISI 5135)

Artem Babaev^{1, a, *}, Nikolai Savchenko^{2, b}, Victor Kozlov^{3, c},
 Artem Semenov^{1, d}, Mikhail Grigoriev^{1, e}



¹ National Research Tomsk State University, 36 Lenin Avenue, Tomsk, 634050, Russian Federation

² Institute of Strength Physics and Materials Science of the Siberian Branch of the Russian Academy of Sciences, 2/4, pr. Akademicheskii, Tomsk, 634055, Russian Federation

³ National Research Tomsk Polytechnic University, 30 Lenin Avenue, Tomsk, 634050, Russian Federation

^a  <https://orcid.org/0000-0003-2334-1679>,  temkams@mail.ru; ^b  <https://orcid.org/0000-0001-8254-5853>,  savnick@ispms.ru;

^c  <https://orcid.org/0000-0001-9351-5713>,  kozlov-viktor@bk.ru; ^d  <https://orcid.org/0000-0002-8663-4877>,  artems2102@yandex.ru;

^e  <https://orcid.org/0009-0009-4214-0312>,  mvgrigoriev@yandex.ru

ARTICLE INFO

Article history:

Received: 21 March 2025

Revised: 10 April 2025

Accepted: 21 April 2025

Available online: 15 June 2025

Keywords:

Oxide ceramics

Turning

Hardened steel

Wear

Funding

The work was carried out within the framework of the state assignment № FSWM-2025-0010 “Physico-chemical regularities of formation of the structural-phase state and physical and mechanical properties of composite ceramic materials resistant to intensive thermomechanical effects and wear”.

ABSTRACT

Introduction. Analysis of contemporary data in the fields of materials science and the application of ceramic cutting tools for machining difficult-to-machine iron- and nickel-based alloys reveals a limited amount of experimental data concerning the use of the promising Y-TZP- Al_2O_3 ceramic, which is based on submicron yttria-partially-stabilized zirconia and reinforced with alumina. **Purpose of the work.** To study the performance of RNGN 120400-01 removable cutting inserts made from Y-TZP- Al_2O_3 ceramic during dry high-speed (200 m/min) cutting of 0.4 C-Cr (AISI 5135) steel (HRC 43...48). **Research Methods.** Characterization of the initial powders and the sintered ceramic, both before and after cutting tests, was performed using X-ray fluorescence (XRF) and X-ray diffraction (XRD) analyses, as well as scanning electron microscopy (SEM) in BSE mode. The physical and mechanical properties of the sintered ceramic were determined using the hydrostatic weighing method, three-point bending, and Vickers microhardness and fracture toughness measurements. Cutting tests were conducted on a high-rigidity lathe in a production shop conditions, involving dry high-speed turning of hardened 0.4C-Cr steel (AISI 5135) (HRC 43...48) in two stages. The first stage involved establishing the allowable variation limits for cutting modes (cutting speed and feed rate) and investigating the wear and failure characteristics of the cutting insert rake and flank faces. The second stage utilized ceramic cutting inserts with a chamfered cutting edge. **Results and discussion.** It was established that for Y-TZP- Al_2O_3 ceramic, the use of cutting modes $V > 200$ m/min, $S > 0.4$ mm/rev, and $t > 0.2$ mm is not advisable due to the short service life of the cutting edge. A chamfer on the cutting edge is necessary to provide controlled edge blunting. The observed wear patterns and analysis of failure areas indicate a dominant brittle fatigue failure mechanism, caused by the thermal effects of high-speed friction combined with tangential stresses from the chip flow. It is concluded that the Y-TZP- Al_2O_3 ceramic composite is promising for use as a cutting tool material for dry high-speed turning of both hardened steels and, potentially, wear-resistant cast irons. Based on the conducted research and described observations, recommendations are formulated for the use of Y-TZP- Al_2O_3 ceramic in future studies.

For citation: Babaev A.S., Savchenko N.L., Kozlov V.N., Semenov A.R., Grigoriev M.V. Performance of Y-TZP- Al_2O_3 composite ceramics in dry high-speed turning of thermally hardened steel 0.4 C-Cr (AISI 5135). *Obrabotka metallov (tekhnologiya, oborudovanie, instrumenty) = Metal Working and Material Science*, 2025, vol. 27, no. 2, pp. 159–173. DOI: 10.17212/1994-6309-2025-27.2-159-173. (In Russian).

Introduction

Ceramics have serious limitations in terms of fracture toughness for structural and some non-structural applications, regardless of their high hardness and modulus of elasticity [1]. However, advances in ceramic production technology have resulted in a new class of ceramic cutting tools with superior characteristics

* Corresponding author

Babaev Artem S., Ph.D. (Engineering)

National Research Tomsk State University,

36 Lenin Avenue, Tomsk,

634050, Russian Federation

Tel.: +7 952 805-09-26, e-mail: temkams@mail.ru

capable of providing productivity intensification [2]. Modern ceramic cutting tools are made in the form of ceramics based on aluminium oxide, zirconium dioxide, cermets, silicon nitride and carbide, *SiAlON*, and others [2].

The martensitic transformation from a metastable tetragonal phase to a stable monoclinic phase creates a stress field around propagating cracks, which is critical to the phenomenon of increasing the fracture toughness of zirconium dioxide ceramics due to phase transformation [3, 4]. Alloying impurities such as Y_2O_3 are commonly added to stabilize the high-temperature tetragonal and/or cubic phase in the microstructure of sintered ceramics [3, 5]. Despite its excellent mechanical properties, the applicability of tetragonal polycrystalline zirconium dioxide (*Y-TZP*) for wear-resistant applications is limited due to its low hardness [5]. However, for example, micro-sized end mills made of *Y-TZP* ceramics have shown the best results among ceramic materials in terms of tool cutting edge sharpness. It is worth noting the reported increase in wear resistance in micro-milling tests using *Y-TZP* tools [6], in which the dimensional effects of cutting edge microgeometry, such as the ratio of the uncut chip thickness to the radius of cutting edge rounding, are known to lead to high mechanical stresses [6].

Ceramic composites with a high hardness using an aluminium oxide matrix with zirconium dioxide inclusions increasing its fracture toughness (*ZTA*) are widely used as ceramic cutting tools for machining hard and wear-resistant materials [2, 7-16]. In [12], high-performance ceramic cutting tools of complex shaped *ZTA* were designed with a chipbreaker and were investigated for the first time. The investigated samples were fabricated using 3D printing based on both photopolymerisation combined with a hot isostatic sintering process. Cutting tools with a relative density of 99.34 %, a *Vickers* hardness of 17.98 ± 0.20 GPa, a bending strength of 779 ± 47 MPa and a fracture toughness of 5.41 ± 0.29 MPa·m^{1/2} were obtained. The effects of three cutting parameters, namely cutting speed, feed rate and depth of cut on cutting tool performance were investigated, and the wear mechanisms of cutting tools were studied. The study published in [13] demonstrates the potential of cutting tools made of *ZTA* composites with *in-situ* formed $SrAl_{12}O_{19}$ as a solution for the woodworking industry, offering an alternative to conventional single carbide tools (*WC+Co* group). The cutting performance and failure mechanisms of *ZTA-MgO* (*ZTA/MgO/MWCNT*) ceramic cutting inserts reinforced with multilayer carbon nanotubes (*MWCNTs*) during continuous dry turning of hardened *AISI 4340* steel (≈ 40 HRC) at high cutting speeds were studied in [14]. *ZTA/MgO/MWCNT* tools showed improved performance compared to *ZTA/MgO* tools, especially in the cutting speed range of 200-300 m/min. The increased microhardness, nanohardness and fracture toughness of *ZTA/MgO/MWCNT* tools contributed to a significant improvement in cutting performance, especially at high cutting speeds, low feed rates and minimum depth of cut. In [15], a new self-lubricating ceramic cutting insert was developed by incorporating 10 wt. % molybdenum (*Mo*) into a *ZTA* composite by pressureless sintering. Temperatures encountered during high-speed turning of *AISI 4340* steel resulted in the formation of thin lubricating tribofilms of *Mo* oxides (MoO_2 and MoO_3) in the contact zone. The self-lubricating properties of the developed insert successfully resisted abrasion and provided an 11 % increase in tool life over common cutting tools. *Singh et al.* [16] studied the machining of *AISI 4340* steel using hot-pressed *ZTA* and *ZTA-CuO* inserts under optimized cutting conditions: cutting speed of 300 m/min, feed rate of 0.16 mm/rev and depth of cut of 0.5 mm. Due to the increased fracture toughness, the *CuO*-reinforced *ZTA* cutting insert achieved longer tool life (20 min) together with a 20 % reduction in wear on the back surface at the end of machining compared to the monolithic insert.

During dry machining, the maximum temperature can exceed 1,000 °C [16]. Most high-speed steels and carbide cutting tools fail under these conditions due to excessive wear, resulting in poor tool life [16]. However, dry machining is a promising approach for economical, efficient and safe machining. Effective implementation of dry machining requires research and evaluation of the cutting process mechanism, cutting tool design and material, and equipment associated with the machining process [2, 15, 17, 18]. Innovations in self-lubricating cutting inserts have positioned dry machining as an attractive manufacturing technology with minimal environmental impact, resulting in a number of positive environmental consequences [15]. Ceramic tools made of *ZTA* ceramics have demonstrated exceptional high-temperature stability, fracture

toughness, chemical stability and impact fatigue strength, as well as increased material removal rates at high temperatures in dry machining [19].

When analyzing the published papers, the lack of information on the cutting properties of $Y-TZP/Al_2O_3$ ceramic composites containing from 5 to 40 wt. % Al_2O_3 draws attention. At the same time, it is known that in comparison with $Y-TZP$ such composites have higher bending strength at room temperature (up to 1,400 MPa), and also retain increased strength at high temperature [4]. The presence of a second phase in the form of Al_2O_3 in $Y-TZP/Al_2O_3$ composites is responsible for an additional strengthening mechanism associated with thermal residual stresses generated by the difference in the thermal expansion coefficient between the two phases [20-22]. The dispersed Al_2O_3 inclusions in the $Y-TZP$ matrix lead to increased hardness, elastic modulus and improved high-temperature mechanical properties, including a high value of fracture toughness [4]. These composites are promising materials for blade machining under extreme conditions [23-25].

The purpose of the present work is to study the behavior of replaceable cutting inserts made of $Y-TZP-Al_2O_3$ ceramics under conditions of dry high-speed (200 m/min) cutting of *AISI 5135* steel (HRC 43-48). In order to achieve the above purpose, the following tasks were solved:

The aim of the present work was to study the behaviour of replaceable cutting inserts made of $Y-TZP-Al_2O_3$ ceramics under conditions of dry high-speed (200 m/min) cutting of *AISI 5135* steel (HRC 43-48). In order to achieve the above aim, the following **tasks were solved**:

- testing of the hypothesis about the possibility of using $Y-TZP-Al_2O_3$ ceramics as a tool material for machining thermally hardened low-alloyed *AISI 5135* steel;
- fabrication and investigation of samples in the form of round ceramic cutting inserts by powder metallurgy methods from commercial powder of *TZ-3Y20AB* grade;
- performance tests in a wide range of cutting modes (speed, feed rate) under conditions of dry high-speed longitudinal turning without impacts;
- establishment of technological limitations on cutting modes when using ceramic cutting inserts, as well as the study of the peculiarities of destruction and wear of contact areas.

Designations

HV , HRC – *Vickers* and *Rockwell* hardness, respectively;

ρ – density, g/cm^3 ;

d_{grain} – grain diameter, μm ;

σ_b – bending strength, MPa;

K_{Ic} – fracture toughness, $MPa \cdot m^{1/2}$;

V – cutting speed, m/min;

S – feed rate, mm/rev;

t – cutting depth, mm;

L – cutting path, mm.

Research methodology

The *AISI 5135* steel blank for testing was made from a round bar with a diameter of 130 mm. The steel blank had a total length of 350 mm. Heat treatment (volume hardening) was performed on conventional modes, taking into account the long holding time in order to uniformly heat the entire blank across the cross-section from the periphery to the future axis of rotation. Heat-treated *AISI 5135* steel was adopted in connection with the set production task on intensification of machining of necks of cutting tool bodies in conditions of LLC “PK MION” (Tomsk). It is also known from the literature that ceramics based on oxide compounds are widely used in cutting of thermally hardened and wear-resistant iron-based alloys [8, 9, 14, 26].

As a raw material for the production of blanks of prototypes of ceramic cutting inserts a commercial powder with the designation *TZ-3Y20AB*, produced by *Tosoh* (Japan) was used. The technological process

of obtaining semi-finished blanks in the form of cylindrical rods with a length of 120 mm included the following technological operations: cold isostatic pressing of powder in a silicone mould at a pressure of 200–300 MPa; preliminary sintering (bisquit firing) in an air environment; rough turning with an outer diameter tolerance of $h9$; final sintering in a vacuum high-temperature furnace; circular grinding to the final size with a diameter tolerance of $h6$; diamond cutting of the rod into blanks with a thickness allowance; flat grinding to the final size in thickness.

Structurally, the cutting insert had a round shape and alphanumeric designation *RNGN 120400-01* according to *GOST 25003-81* “Ceramic indexable throw-away inserts for cutting tools. Specifications”, which corresponds to a thickness of 4.76 mm and a diameter of 12.70 mm without additional chamfers and ledges on the rake surface. A total of 5 (five) cutting inserts were produced, the faces of each insert was pre-grounded on a surface grinding machine mod. *3D711AF11* using diamond wheel *IAI 250×20×5×5×76 AC4 125/100 100% B2-01*, special multi-place tooling and abundant supply of water-based coolant. Visual inspection for the presence of surface cracks was performed using a magnifying glass with magnification $20\times$, and random inspection was carried out in the process of evaluating the initial condition of the cutting inserts on a scanning electron microscope at magnifications $500\times$ and more (Fig. 1).



Fig. 1. Ceramic inserts (a) and electron microscopy of the cutting edge (b) in the initial state



Fig. 2. Mandrel with a ceramic insert attached

The ceramic cutting inserts were mounted in the *CRDNN 2525M 12-ID* holder by *Sandvik Coromant (Switzerland)* using a carbide pad by pressing from above (Fig. 2).

The initial ceramic powders and sintered products were studied using certified equipment. Elemental composition was determined on X-ray fluorescence wave dispersive spectrometer *XRF-1800 mod. XRF-1800* by *Shimadzu (Japan)*. The appearance of powders and their particle size distribution were studied on a scanning electron microscope mod. *Mira 3LMU* by *Tescan (Czech Republic)*. X-ray structural analysis was carried out on X-ray diffractometer mod. *DRON 8N* from *JSC “IC “Burevestnik” (St. Petersburg)*, equipped with a microstrip X-ray detector mod. *Mythen 2R 1D* by *Dectris (Japan)*. X-ray images were taken with $CuK\alpha$ -radiation ($\lambda = 0.15406$ nm) in the range of angles 2θ 20–90°. The detector scanning step was 0.1° and the data acquisition time was 30 s. The specific surface area of the initial powders was determined on the device mod. *SORBI-M of LLC “META” (Novosibirsk)*, by nitrogen adsorption by the 4-point *Brunauer-Emmett-Taylor* method (theory of polymolecular adsorption).

The bulk area of powders was determined by measuring the volume of powder of known mass in a graduated cylindrical vessel.

After sintering, the representative samples were ground on a diamond wheel and polished using standard metallographic technology. The density of the samples after sintering was measured by hydrostatic weighing. The average grain size of sintered samples was calculated by the secant method using optical photographs of the thermally etched surface. The strength was determined by the method of three-point bending of ground specimens of $4 \pm 0,1 \times 3 \pm 0,1 \times 40$ mm using a compression testing machine (hydraulic press) manufactured by LLC "NIKTSIM Tochmashpribor" (Armavir). Evaluation of microhardness HV and crack resistance KIc was carried out on a universal hardness tester mod. *Duramin-500* by *Stuers A/S* (Denmark) with an automatic force sensor by indenting the polished surface with a *Vickers* pyramid at a load of 98.07 N. The length of the indentation diagonals and the extent of cracks for the calculation of microhardness and fracture toughness were evaluated using an optical microscope.

The ceramic inserts were tested during cutting on a *MULTUS B300-W* lathe made by *Okuma* (Japan) in the body cutting tool production shop of LLC "PK MION" (Tomsk, Russia) (Fig. 3). The workpiece was clamped in a hydraulic chuck by the tail section, which was coaxial with the machined surface and had a diameter of 70 mm and a length of 50 mm.

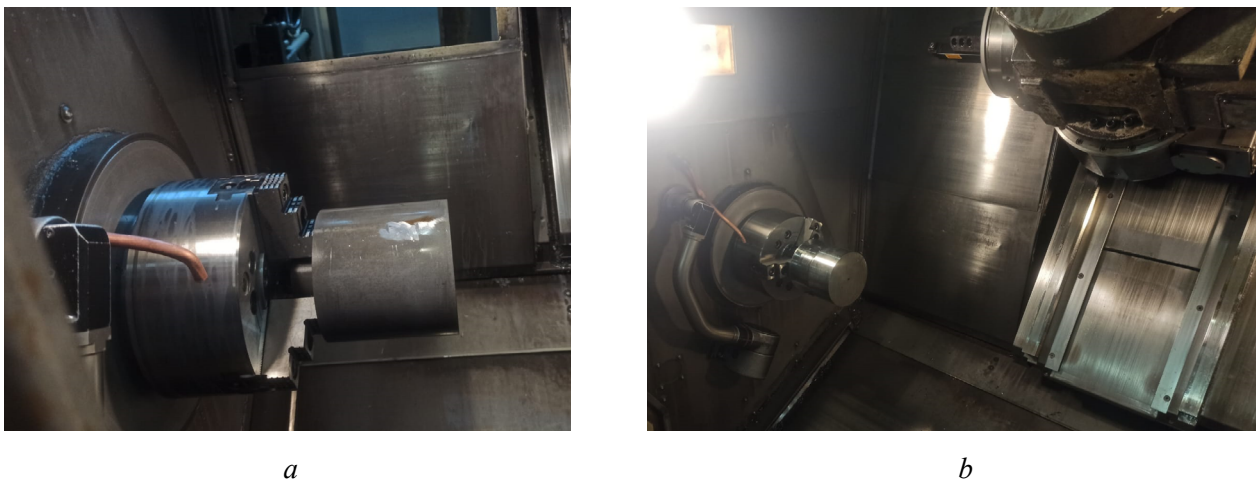


Fig. 3. Views of the machine tool working area with a fixed workpiece (a) and the mandrel (b) with a ceramic insert

Performance tests of ceramic cutting inserts were carried out in two stages. All tests were carried out during longitudinal turning without impacts in dry conditions. When the cutting edge chipped, the insert was rotated by $\approx 30^\circ$ or flipped to the opposite side. Cutting modes were taken from sources [2, 6–8, 12, 14, 15, 26]. The cutting path at which chip formation is observed was taken as a criterion of tool performance. The onset of failure indicated brittle fracture of the cutting edge and cessation of chip formation.

In the first test phase, ceramic inserts with cutting edges without additional processing were used, i.e. the microgeometry was generated in a flat grinding process. To establish the limits of permissible variation of modes during turning we used the following values: cutting speed $V = 200; 300; 400$ m/min; feed rate $S = 0.05; 0.1; 0.2; 0.4; 1.0$ mm/rev; depth of cut $t = 0.1; 0.2; 0.4$ mm.

At the second stage, the performance was tested at constant modes: $V = 200$ m/min; $S = 0.25$ mm/rev; $t = 0.1$ mm. At the same time, an insert with a chamfer of $0.2 \times 45^\circ$ mm formed on the cutting edge was used.

Results and discussion

The chemical composition of *AISI 5135* steel complies with *GOST 4543-2016* "Structural alloy steel production. Specifications". In the initial state, *AISI 5135* steel has a ferrite-perlite structure, and hardness is *HRC* 21–26, and after quenching – martensite with residual austenite (5–8 %). Hardness measurements of the quenched steel showed that there are variations in the *HRC* 43–48 range along the cross-section depth.

The elemental composition of the initial ceramic powder is given in Table 1.

The measurements showed that the actual particle size of the ceramic powder was in the range of 0.04–0.09 μm and the specific surface area was $15 \pm 3 \text{ m}^2/\text{g}$.

The results of measurements of physical and mechanical properties carried out on representative specimens are presented in Table 2.

Table 1

Chemical composition of TZ-3Y20AB ceramic powder

Mass fraction of chemical compounds, %					
Y_2O_3	Al_2O_3	SiO_2	Fe_2O_3	Na_2O	ZrO_2
3.9 ± 0.3	19 ± 1	< 0.02	< 0.01	< 0.04	balance

Table 2

Physical and mechanical properties of sintered Y-TZP- Al_2O_3 ceramic

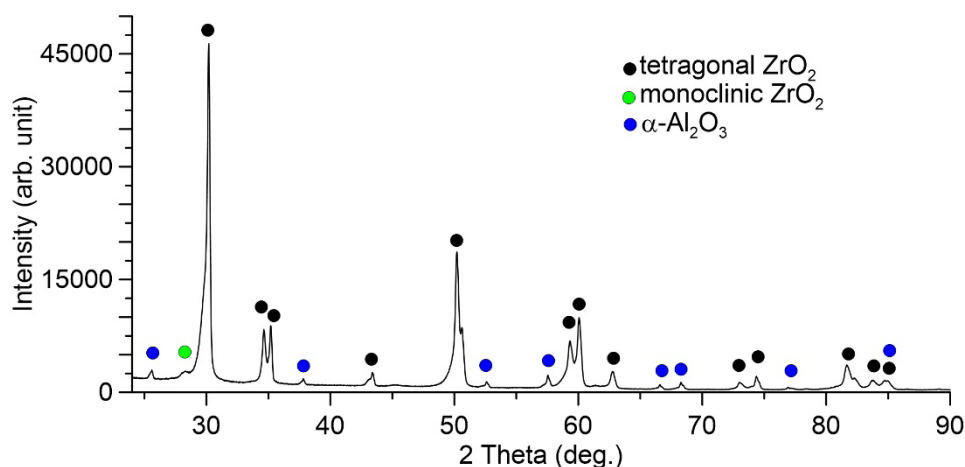
Density ρ (g/cm^3)	Grain diameter d_g (μm)	Bending strength (MPa)	Microhardness $HV10$ (GPa)	Fracture toughness K_{Ic} ($\text{MPa} \cdot \text{m}^{1/2}$)
5.5 ± 0.2	0.4 ± 0.09	1200 ± 160	14 ± 0.6	7.2 ± 0.4

The phase composition of the ground surface of the sintered Y-TZP- Al_2O_3 ceramics is shown in Fig. 4. It can be seen that the main phases are the matrix phase of tetragonal ZrO_2 and the strengthening phase of $\alpha\text{-}Al_2O_3$. A small amount of monoclinic ZrO_2 ($\approx 3 \text{ vol.}\%$) could appear due to grinding of the surface of the ceramic inserts, when a phase transition from the metastable tetragonal to the stable monoclinic phase occurs under load.

The results of observations of the process of dry turning with ceramic cutting inserts are presented and described below. The modes were varied according to the data specified in Table 3.

It was noted that, regardless of feed rate and cutting depth, at a cutting speed of 200 m/min, a spiral chip with traces of whiteness is formed with periodic appearance of burning chips, and in the speed range from 300 to 400 m/min, the chip consists of individual fragments, the intensive combustion of which during cutting is accompanied by a sheaf of sparks (Fig. 5).

Let us consider in detail the wear characteristics of the working surfaces that form the cutting edges of ceramic inserts. Characteristic patterns of wear and destruction of the working surfaces of the cutting edges are shown in Fig. 6.


 Fig. 4. X-ray diffraction pattern of Y-TZP- Al_2O_3 composite ceramic

Results of tests in stage 1

No.	Cutting speed V (m/min)	Feed rate S (mm/rev)	Cutting depth t (mm)	Cutting distance L^* (mm)	Note
1	200	0.05	0.2	50	edge chipping, chip burning
2	300		0.4	5	
3	400		0.1	10	
4		50		edge chipping, oxidized chip	
5	200	0.4	60		10
6	600	0.25	0.1	50	edge chipping, increased vibrations
7				10	edge chipping, low surface roughness
8				50	
9	100	0.1	100	edge chipping	
10	200	0.4	600		
11**	200	0.25			edge chipping

* L – path until catastrophic wear (cessation of chip formation)

** – data from 4 repetitions.

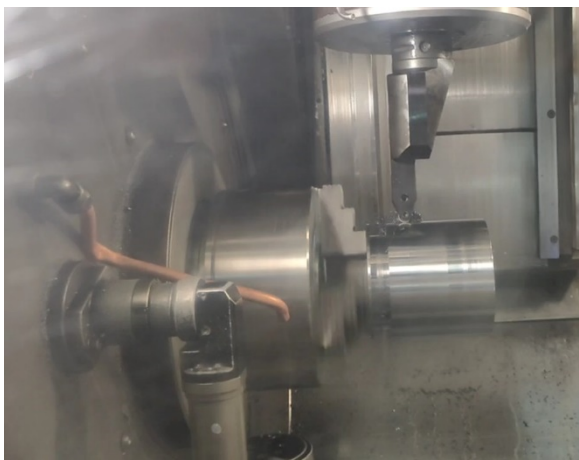
*a**b*

Fig. 5. Cutting process fragment with the formation of spiral (*a*) and burning (*b*) chips at cutting speeds of 200 and 400 m/min, respectively

After the expected wear value had been reached, when the cessation of chip formation due to chipping was visually recorded, the insert was rotated clockwise, which made it possible to observe different stages of wear on the same cutting insert (Fig. 6, *a*, zone 1), i.e. the right part of the worn surface was rotated clockwise (Fig. 6, *a*, zone 2). The wear of the cutting insert begins to manifest itself in the form of a crater up to 1.1 mm long (Fig. 6, *a*, zone 1) on the rake surface. It is closely adjacent to the cutting edge and goes over to the main back surface (Fig. 6, *a*, zone 1). In this case, it is not so much wear that occurs (therefore, it is generally incorrect to speak about wear), as brittle fracture (delamination) of a radial shape along surfaces parallel to the rake surface. This is due to the action of tangential stresses, the greatest value of which is located slightly below the rake surface [26]. The zone of delamination of the cutting material passes far

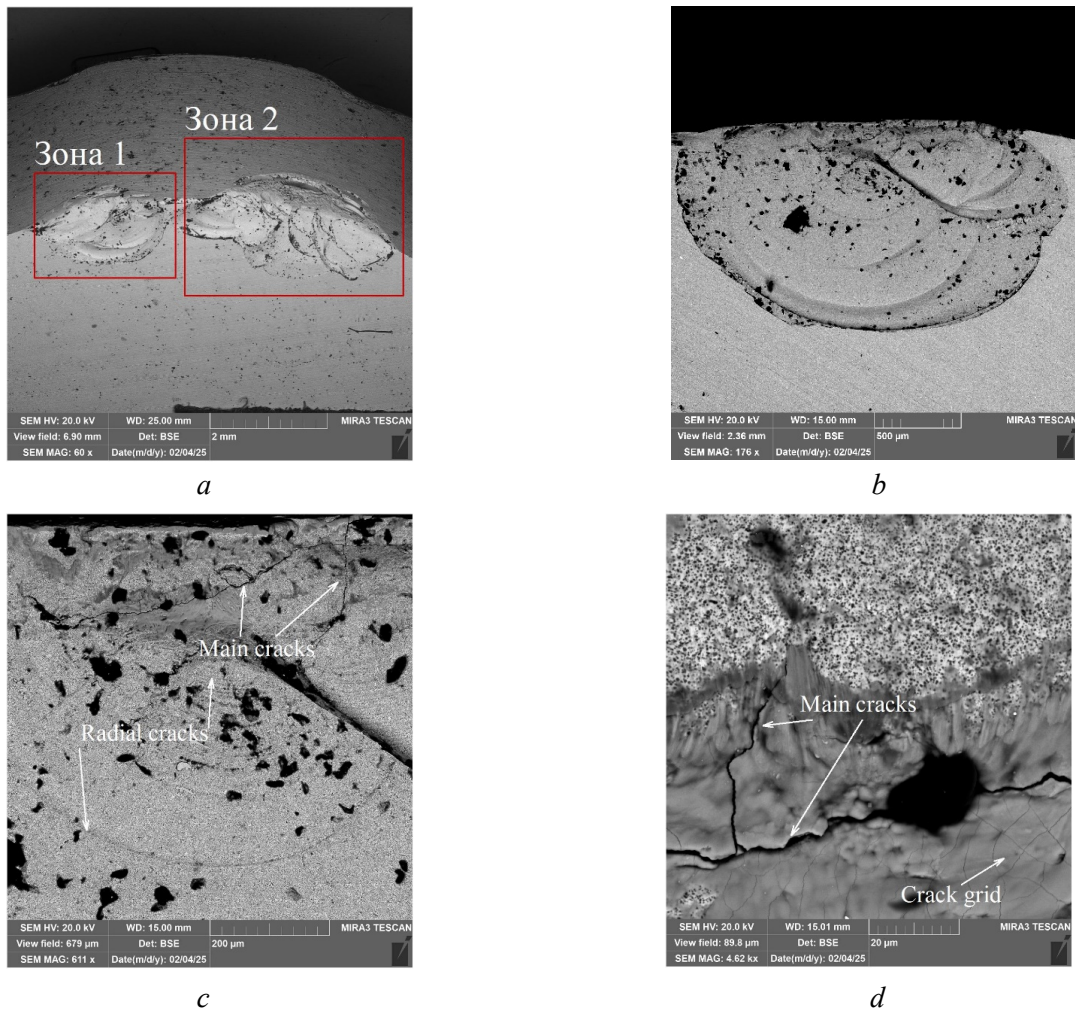


Fig. 6. Typical micrographs of wear and failure areas of ceramic cutting inserts without cutting edge preparation:

a – general view; *b, c* – crater on the rake face; *d* – major cracks

beyond the line of the chip contact length with the cutting insert, therefore, no traces of chip contact with the rake surface are observed.

As a result of tool material fatigue due to periodic twitching and tearing of the contact surface of the chip near the cutting edge, defects accumulate, which develop first into a micro- and then into a macro-crack running parallel to the rake surface. This macro-crack even extends to the back surface, although the relief of the resulting micro-crater indicates a predominant crack development towards the rake surface.

There is no adhesion of the machined material on the rake surface, indicating a low coefficient of friction in this area (which is typical for ceramic cutting materials) and no adhesion beyond the brittle fracture region. No traces of abrasive wear are also observed, which is due to the high hardness of the tool material.

The microcrater surface is also free of particles of the workpiece material, although its relief contributes to their retention (Fig. 6, *a*, zone 1). This indicates high shear strength of the near-cutting part of the chip, or at least that the shear strength there is greater than the contact tangential stresses on the chip-tool surface. When the micro-crater increases to 1.2 mm (Fig. 6, *a*, zone 2), additional delamination of the tool material occurs, i.e., several radial micro-craters are formed. Here, particles of the workpiece material are observed in stagnant zones, although in very small volumes. In our opinion, this is due to the increase in the depth of these zones, which contributes to its retention in the form of micro-particles. At high magnification, small particles (a black spot of about 0.15 mm) of the workpiece material can be seen on the micro-crater surface (Fig. 6, *b*). Although the micro-crater surface has a basic radial shape, it also contains additional lines of brittle delamination of a complex shape. At even greater magnification (Fig. 6, *c*), deep main cracks

can be seen on the surface of the micro-crater near the cutting edge, already passing perpendicular to the rake surface. Their character indicates their thermal nature: near the cutting edge, the insert heats up much faster and more than when moving away from it, which leads to the appearance of thermal micro-cracks. At magnification (Fig. 6, *d*), a black cavity is observed on the surface of the micro-crater, which indicates the tearing out of a ceramic particle of about 20 μm in size. A thermal crack passing through this area indicates a possible weakening of the tool material due to a sharp temperature drop.

Let us consider some features of wear of ceramic cutting inserts on which a chamfer was forcibly formed (Table 4).

On the contact surfaces of the cutting insert, areas without traces of significant wear are recorded, and minor adherence of the workpiece material is observed only near the cutting edge (Fig. 7, *a*). No traces of abrasive wear are observed. In this regard, it seems advisable to continue research in the part of using $Y\text{-TZP-Al}_2\text{O}_3$ cutting ceramics for dry high-speed turning and milling of hardened and difficult-to-machine materials, as well as to conduct research on comparative resistance tests with a study of the roughness of the workpiece surfaces.

Table 4

Results of tests in stage 2

No.	Cutting speed V (m/min)	Feed rate S (mm/rev)	Cutting depth t (mm)	Cutting distance L^* (mm)	Note
1	200	0.25	0.1	3300	no edge chipping, oxidized chip

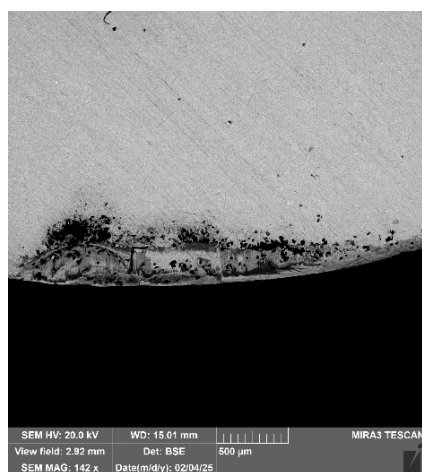
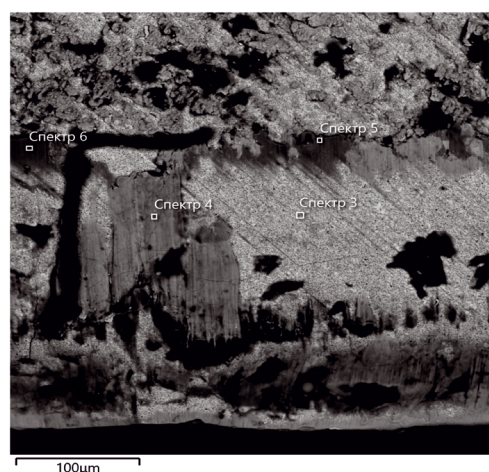
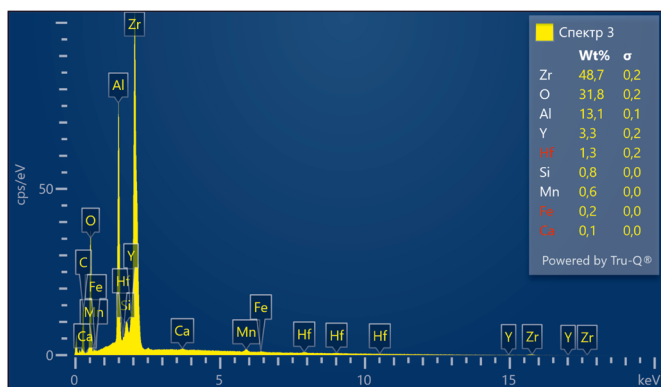
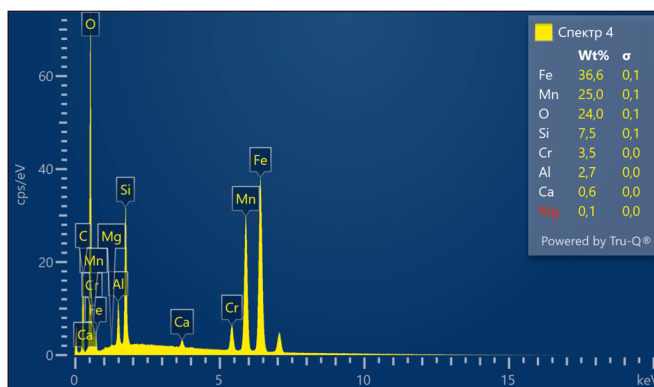
*a**b**c**d*

Fig. 7. Typical micrographs of wear and failure areas of ceramic cutting inserts with a chamfered cutting edge: *a* – general view; *b* – crater on the rake face; *c*, *d* – elemental mapping

Conclusions

1. Performance tests have shown the promising use of ceramic powder of *TZ-3Y20AB* (*Y-TZP-Al₂O₃*) grade, obtained by the technology of cold isostatic pressing followed by high temperature free sintering, for manufacturing of cutting inserts *RNGN 120400-01* for turning hardened steel *AISI 5135* (*HRC 43–48*).

2. It is not advisable to use the following cutting modes due to the short-term operation of the cutting edge of the cutting insert: $V > 200$ m/min; $S > 0.4$ mm/rev; $t > 0.2$ mm. The use of an insert with a blunt edge ensures stable turning on a cutting path of at least 3,300 mm when using the following cutting modes: $V = 200$ m/min; $S = 0.25$ mm/rev; $t = 0.1$ mm

3. Electron microscopy of wear and fracture sites demonstrates the dominant mechanism of brittle fatigue fracture caused by the thermal cycling effect of friction and tangential stresses in the cutting region.

4. The *Y-TZP-Al₂O₃* ceramic composition is suitable for use as a tool material intended for dry high-speed turning of heat-treated steels of increased hardness. However, it is necessary to conduct comprehensive studies formalizing the effect of machining modes on the durability and roughness of machined surfaces both when cutting hard steels and wear-resistant cast irons.

References

1. Basu B. Toughening of yttria-stabilised tetragonal zirconia ceramics. *International Materials Reviews*, 2005, vol. 50 (4), pp. 239–256. DOI: 10.1179/174328005X41113.
2. Patel H., Patil H. Tribological performance based machinability investigations of Al_2O_3 - ZrO_2 ceramic cutting tool in dry machining of Ti-6Al-4V alloy. *Tribology International*, 2022, vol. 176, p. 107776. DOI: 10.1016/j.triboint.2022.107776.
3. Perry C., Liu D., Ingel R.P. Phase characterization of partially stabilized zirconia by Raman spectroscopy. *Journal of the American Ceramic Society*, 1985, vol. 68 (8), pp. C-184–C-187. DOI: 10.1111/j.1151-2916.1985.tb10176.x.
4. Nettlehip I., Stevens R. Tetragonal zirconia polycrystal (TZP) – A review. *International Journal of High Technology Ceramics*, 1987, vol. 3, pp. 1–32. DOI: 10.1016/0267-3762(87)90060-9.
5. Arin M., Goller G., Vleugels J., Vanmeensel K. Production and characterization of ZrO_2 ceramics and composites to be used for hip prosthesis. *Journal of Materials Science*, 2008, vol. 43 (5), pp. 1599–1611. DOI: 10.1007/s10853-007-2343-x.
6. Mayer T., Kieren-Ehse S., Kirsch B., Aurich J.C. Comparison of different 3Y-TZP substrates for the manufacture of all-ceramic micro end mills with respect to the cutting edge radius and the tool wear. *Manufacturing Letters*, 2023, vol. 38, pp. 44–46. DOI: 10.1016/j.mfglet.2023.09.001.
7. Dyatlova Ya.G., Kovelonov N.Yu., Rumyantsev V.I., Ordanyan S.S. Novaya rezhushchaya keramika v sisteme Al_2O_3 - ZrO_2 (Y_2O_3)-Ti(C,N) [New cutting $Al_2O_3/ZrO_2/Ti(C,N)$ ceramics]. *Metaloobrabotka = Metalworking*, 2014, no. 1 (79), pp. 32–36.
8. Senthil Kumar A., Raja Durai A., Sornakumar T. Machinability of hardened steel using alumina based ceramic cutting tools. *International Journal of Refractory Metals and Hard Materials*, 2003, vol. 21 (3–4), pp. 109–117. DOI: 10.1016/S0263-4368(03)00004-0.
9. Basha M.M., Basha S.M., Singh B.K., Mandal N., Sankar M.R. A review on synthesis of zirconia toughened alumina (ZTA) for cutting tool applications. *Materials Today: Proceedings*, 2020, vol. 26, pt. 2, pp. 534–541. DOI: 10.1016/j.matpr.2019.12.134.
10. Smuk B., Szutkowska M., Walter J. Alumina ceramics with partially stabilized zirconia for cutting tools. *Journal of Materials Processing Technology*, 2003, vol. 133, pp. 195–198. DOI: 10.1016/S0924-0136(02)00232-7.
11. Liang X., Liu Z., Liu W., Li X. Sustainability assessment of dry turning Ti-6Al-4V employing uncoated cemented carbide tools as clean manufacturing process. *Journal of Cleaner Production*, 2019, vol. 214, pp. 279–289. DOI: 10.1016/j.jclepro.2018.12.196.
12. Liu W., Wu H., Xu Y., Lin L., Li Y., Wu S. Cutting performance and wear mechanism of zirconia toughened alumina ceramic cutting tools formed by vat photopolymerization-based 3D printing. *Ceramics International*, 2023, vol. 49 (14), pt. A, pp. 23238–23247. DOI: 10.1016/j.ceramint.2023.04.153.



13. Thakur T., Heinen S., Ehrle B., Blugan G. Optimizing woodcutting with zirconia-toughened alumina: processing, performance, and industrial insights. *Heliyon*, 2025, vol. 11 (2), p. e41785. DOI: 10.1016/j.heliyon.2025.e41785.
14. Prajapati P.K., Bapanapalle C.O., Biswas P., Kumar Sadhu K., Ranjan Sahoo R., Mandal N. Cutting performance, failure mechanisms and tribological properties of MWCNT-reinforced ZTA-MgO ceramic inserts in high-speed machining of hardened AISI-4340 steel. *Diamond & Related Materials*, 2024, vol. 153, p. 112094. DOI: 10.1016/j.diamond.2025.112094.
15. Ghosh K., Goswami S., Kumar Prajapati P., Roy P., Mandal N. Pressure-less sintering of molybdenum-reinforced ceramic cutting inserts with improved tool life. *International Journal of Refractory Metals and Hard Materials*, 2024, vol. 120, p. 106619. DOI: 10.1016/j.ijrmhm.2024.106619.
16. Singh B.K., Goswami S., Ghosh K., Roy H., Mandal N. Performance evaluation of self lubricating CuO added ZTA ceramic inserts in dry turning application. *International Journal of Refractory Metals and Hard Materials*, 2021, vol. 98, p. 105551. DOI: 10.1016/j.ijrmhm.2021.105551.
17. Wang B., Liu Z. Influences of tool structure, tool material and tool wear on machined surface integrity during turning and milling of titanium and nickel alloys: a review. *The International Journal of Advanced Manufacturing Technology*, 2018, vol. 98 (5–8), pp. 1925–1975. DOI: 10.1007/s00170-018-2314-1.
18. Wang Z.G., Wong Y.S., Rahman M. High-speed milling of titanium alloys using binderless CBN tools. *International Journal of Machine Tools and Manufacture*, 2005, vol. 45, pp. 105–114. DOI: 10.1016/j.ijmachtools.2004.06.021.
19. Sun F.J., Qu S.G., Pan Y.X., Li X.Q., Li F.L. Effects of cutting parameters on dry machining Ti-6Al-4V alloy with ultra-hard tools. *The International Journal of Advanced Manufacturing Technology*, 2015, vol. 79 (1–4), pp. 351–360. DOI: 10.1007/s00170-014-6717-3.
20. Bichaud E., Chaix J.M., Carry C., Kleitz M., Steil M.C. Flash sintering incubation in Al₂O₃/TZP composites. *Journal of the European Ceramic Society*, 2015, vol. 35 (9), pp. 2587–2592. DOI: 10.1016/j.jeurceramsoc.2015.02.033.
21. Muccillo R., Muccillo E.N.S. Electric field-assisted flash sintering of tin dioxide. *Journal of the European Ceramic Society*, 2014, vol. 34 (4), pp. 915–923. DOI: 10.1016/j.jeurceramsoc.2013.09.017.
22. Yoshida H., Sakka Y., Yamamoto T., Lebrun J-M., Raj R. Densification behaviour and microstructural development in undoped yttria prepared by flash-sintering. *Journal of the European Ceramic Society*, 2014, vol. 34 (4), pp. 991–1000. DOI: 10.1016/j.jeurceramsoc.2013.10.031.
23. Srdić V.V., Winterer M., Hahn H. Sintering behavior of nanocrystalline zirconia doped with alumina prepared by chemical vapor synthesis. *Journal of the American Ceramic Society*, 2000, vol. 83, p. 1853. DOI: 10.1111/j.1151-2916.2000.tb01481.x.
24. Sakka Y., Suzuki T.S., Morita K., Nakano K., Hiraga K. Colloidal processing and superplastic properties of zirconia-and alumina-based nanocomposites. *Scripta Materialia*, 2001, vol. 44, p. 2075. DOI: 10.1016/S1359-6462(01)00889-2.
25. Rana R.P., Pratihari S.K., Bhattacharyya S. Powder processing and densification behaviour of alumina–high zirconia nanocomposites using chloride precursor. *Journal of Materials Processing Technology*, 2007, vol. 190 (1–3), pp. 350–357. DOI: 10.1016/j.jmatprotec.2007.02.009.
26. Kozlov V., Zhang J.Y., Guo Y.B., Sabavath S.K. Research of contact stresses distribution on plunge-cutting into a steel workpiece. *Key Engineering Materials*, 2018, vol. 769, pp. 284–289. DOI: 10.4028/www.scientific.net/KEM.769.284.

Conflicts of Interest

The authors declare no conflict of interest.

